Published in final edited form as:
Atherosclerosis. 2014 April ; 233(2): 682–690. doi:10.1016/j.atherosclerosis.2014.01.056.

Effect of shear stress on water and LDL transport through cultured endothelial cell monolayers

Hongyan Kang[1,2], **Limary M. Cancel**[2], and **John M. Tarbell**[2,*]

[1]Key Laboratory for Biomechanics and Mechanobiology of Ministry of Education, School of Biological Science and Medical Engineering, Beihang University, Beijing, China

[2]Department of Biomedical Engineering, The City College of The City University of New York, New York, USA

Abstract

Previous animal experiments have shown that the transport of LDL into arterial walls is shear stress dependent. However, little work has probed shear effects on LDL transport in vitro where conditions are well defined and mechanisms are more easily explored. Therefore, we measured shear induced water and LDL fluxes across cultured bovine aortic endothelial (BAEC) monolayers in vitro and developed a three-pore model to describe the transport dynamics. Cell apoptosis was quantified by TdT-mediated dUTP nick end labeling (TUNEL) assay. We also examined the role of nitric oxide (NO) in shear induced water and LDL fluxes by incubating BAEC monolayers with a NO synthase inhibitor, N^G-monomethyl-L-arginine (L-NMMA). Our results show that direct exposure of endothelial monolayers to 12 dyn/cm^2 shear stress for 3 hours elicited a 2.37-fold increase in water flux (J_v), a 3.00-fold increase in LDL permeability (P_e), a 1.32-fold increase in LDL uptake, and a 1.68-fold increase in apoptotic rate. L-NMMA treatment of BAEC monolayers blocked shear induced J_v response, but had no significant effect on shear responses of P_e and cell apoptosis. A long time shear exposure (12 h) of endothelial monolayers reduced P_e and apoptotic rate close to the baseline. These results suggest that an acute change in shear stress from a static baseline state induces increases in water flux that are mediated by a NO dependent mechanism. On the other hand, the permeability of endothelial monolayers to LDL is enhanced by a short term-shear application and reduced nearly to the baseline level by a longer time shear exposure, positively correlated to the leaky junctions forming around apoptotic cells.

Keywords

shear stress; LDL permeability; water flux; bovine aortic endothelial cells; leaky junctions

1. Introduction

A principal function of endothelial cells is the regulation of fluid and solute transport into the arterial wall and the underlying tissue. The ease of fluid transport across the endothelium is described by the hydraulic conductivity (L_p), and changes in L_p likely correlate with the

*Corresponding Author: Dr. John M. Tarbell, Department of Biomedical Engineering, The City College of The City University of New York, Steinman Hall Room T403H, 140th Street and Convent Avenue, New York, NY10031, USA. Tel.: +1 212 650 6841; Fax: +1 212 650 6727; tarbell@ccny.cuny.edu.

movement of water-soluble solutes (25). Hemodynamic factors, fluid flow induced shear stress in particular, mediate the regulation of L_p as first demonstrated in vitro by Sill et al (34). Using the same bovine aortic endothelial cell (BAEC) monolayer model, Chang et al. (7) showed that shear-induced increases in hydraulic conductivity are mediated by nitric oxide (NO) production since the increases in L_p could be completely blocked by a NO synthase (NOS) inhibitor. A similar phenomenon has also been displayed in bovine retinal microvascular endothelial cells (BRECs). Lakshminarayanan et al. (20) found that a 14.6-fold increase of L_p in response to 20 dyn/cm^2 step change could be significantly attenuated by a preincubation of the BRECs with a NOS inhibitor, L-NMMA. These findings are consistent with in vivo studies. Williams (37, 41) measured L_p after step changes in shear stress in arterioles, true capillaries, and venules of the frog mesentery using the modified Landis technique. The response of the vessels varied across the capillary bed, with arteriolar capillaries showing no response of L_p while true and venular capillary L_p were related to the magnitude of the shear stress stimulus. A recent in vivo study performed in autoperfused microvessels in rat mesentery also indicated that changes in L_p were positively correlated with the magnitude of acute changes in shear stress (19). However, controversy remains as Adamson et al. (1) measured L_p in rat mesenteric venular microvessels and observed that microvascular permeability to water is independent of shear stress but dependent on flow direction.

As indicated above, acute changes in shear stress regulated water transport via a NO dependent mechanism in many previous studies. The transport of water-soluble macromolecules, such as low density lipoprotein (LDL), through the arterial wall could also be affected by shear stress. Excess LDL filtration and accumulation in the subendothelial space are important events in early atherogenesis (33). It has been well established that there are three pathways for LDL transport across the endothelium: transcytosis in vesicles, paracellular transport through the breaks in the tight junction strand and leaky junctions associated with cell turnover or apoptosis (36). A number of studies, including in vivo (21, 22), in vitro (4–6), and theoretical investigations (39), have shown that leaky junctions associated with dying or dividing cells are the dominant pathway for LDL transport. In studies by Cancel et al., leaky junctions accounted for 90.9% of LDL transport under convective conditions, with leaky junctions being closely associated with apoptotic cells (4, 5).

Using the trapped ligand method, Berceli et al. (2) examined the incorporation and degradation rates of LDL at the rabbit aorto-iliac bifurcation in three regions of distinct flow patterns: flow separation, transitional, and unidirectional flow. They showed that both the accumulation and degradation were greater in the flow separation region with low shear stress. This finding is consistent with a later numerical study reported by Buchanan et al. (3), performed by correlating hemodynamic parameters with sites of elevated LDL permeability around the rabbit aorto-celiac branch in vivo. Most recently, Olgac et al. (27) developed a novel modeling method of LDL transport in a stenosed coronary artery, taking into account the effects of local wall shear stress on the endothelial layer and the pathways of water and solute fluxes by a three pore model, and predicted increased permeablility of solutes in low shear stress regions because of the presence of a larger number of leaky junctions compared with high shear stress regions. Previous in vitro studies focusing on the effects of shear stress on LDL uptake into (not across) endothelial cells have shown that imposition of shear stress to BAECs (35), EC-SMC cocultures (26), or ECV304 cells (38) enhances LDL uptake by the cells. All of these studies have highlighted the importance of shear effects on LDL transport. However, no studies have probed the effect of shear stress on LDL transport across cultured endothelial cell monolayers in vitro under well controlled conditions.

In this study we investigated effects of steady shear stress on water and LDL transport simultaneously, using the same BAEC model and shear apparatus previously employed to study the effect of shear stress on L_p by Lopez-Quintero et al (23). We also examined the effect of shear on apoptosis rates, and the role of NO on shear-induced changes in LDL and water transport and apoptosis.

2. Materials and methods

2.1. Cell culture

BAECs were purchased from Lonza Inc. (Walkersville, MD). Cells were grown in T-25 flasks in endothelial cell growth media supplemented with 5% FBS and growth factors (Lonza, Walkersville, MD). The flasks were kept at 37°C and 5% CO_2. The medium was changed every 2 days. For the transport experiments, cells were plated at a density of 10^4 cells/cm^2 on Transwell polyester filters (Corning, Acton, MA) with 0.4 μm pores which were previously coated with 30 μg/ml fibronectin (Sigma Chemical, St. Louis, MO). Experiments were run 5–7 days after plating, when the cells reached confluence but were free from overgrowth. Cells were used from passages 4 to 7, similar to our previous study (5). However, note that the cells used in the previous study were purchased from a different source (VEC Technologies Inc.) and grown in different medium.

2.2 Measurement of water and LDL flux

A custom made transport system previously developed in our lab and extensively described was used to measure both water and solute flux simultaneously (4–6, 23). Briefly, the filter covered with a monolayer of cells was sealed in a chamber to form a luminal compartment and an abluminal compartment. The abluminal compartment was connected to a fluid reservoir via Tygon and borosilicate glass tubing. The height of the reservoir could be adjusted to apply a hydrostatic pressure differential across the EC monolayer. When 10 cm H_2O hydrostatic pressure was applied, the water flux (J_v) was recorded by tracking the position of an air bubble which had been inserted into a glass capillary connected to the chamber's outflow line. To test the accuracy of the volume recorded by the bubble tracker, the fluid reservoir was replaced with a calibrated pipette capable of measuring volume in increments of 10 μL. When volumes in the range of 10 to 80 μL were measured, the bubble tracker recorded volumes within the margin of error of our calibrated pipette (5 μL). During a typical 4-hour experiment, about 35 μL of water are transported through the cell monolayer. The LDL flux was determined by measuring the concentration of 1,1′-dioctadecyl-3,3,3′,3′-tetramethyl-indocarbocyanine labeled LDL (DiI-LDL) (Biomedical Technologies, Stoughton, MA) in the abluminal chamber using an automated fluorometer system consisting of a laser excitation source, an emission detector, optical fibers, a photomultiplier and the FluorMeasure data acquisition program (C&L Instruments, Hummelstown, PA).

2.3. Shear stress application

A rotating disk device was used to apply shear stress. The disk was set at a height (h) of 500 μm from the monolayer surface. The speed of the shear rod was ramped up from zero to its final value over one minute, after which it remained constant to provide a steady flow. The shear level could be defined by $\tau = \mu \times \omega \times r/h$, where μ is the viscosity of the medium, ω is the rotational speed and r is the radius of the disk. The maximum shear level at the edge of the disk was adjusted to 12 dyn/cm^2. The average shear stress over the entire filter was two-thirds of the maximum. To drive a physiological amount of water flux across the cell monolayer, a 10 cm H_2O hydrostatic pressure differential was applied at time zero for 1 hr of sealing then shear stress was applied while J_v and P_e were simultaneously measured.

2.4. VE-cadherin immunostaining

At the end of certain experiments, BAEC monolayers were washed twice with DPBS, fixed in 1% paraformaldehyde for 10 min, permeabilized with 0.2% Triton X-100 for 10 min and blocked in 10% goat serum and 0.1% Triton X-100 for 1 hour at room temperature. After washing with DPBS, BAEC monolayers were incubated with VE-cadherin antibody (rabbit polyclonal antibody, Cell Signaling Technology, Danvers, MA) overnight at 4 °C. Afterwards, cells were washed 5 times and incubated with Alexa Fluor 488 goat anti rabbit IgG (Invitrogen, Carlsbad, CA) for 1h at room temperature. The monolayers were washed 4 times and imaged under a Nikon Eclipse TE2000-E microscope coupled with a Photometric Cascade 650 CCD camera (Roper Scientific, Tucson, AZ), or with a Zeiss LSM 510 confocal microscope.

2.5. TUNEL assay

The apoptotic rates of BAEC monolayers were measured by the TdT-mediated dUTP nick end labeling (TUNEL) technique using the in situ cell death detection kit (TMR red) from Roche (Indianapolis, IN). After transport experiments, the filters were fixed in 4% paraformaldehyde for 1h, then rinsed with DPBS and incubated with fresh blocking solution (3% H_2O_2 in methanol) for 10 min. Cells were permeabilized with 0.1% triton X-100 in 0.1% sodium citrate for 2 min and incubated with TUNEL reaction mixture for 1 h at 37 °C. After washing with DPBS 3 times, the monolayers were incubated with DAPI solution for 5 min and analyzed under a fluorescent microscope in a dark room. The apoptosis rate was defined as the number of apoptotic cells (TMR red positive) divided by the total cell number of that field and presented as a percent.

2.6. L-NMMA treatment

In order to determine the role of nitric oxide in shear induced water and LDL flux, 50 μM N^G-monomethyl-L-arginine (L-NMMA) (Sigma Chemical, St. Louis, MO) (7) was added on the luminal side of the BAEC monolayers at the beginning of the experiment to inhibit the activity of nitric oxide synthase (NOS). Paired monolayers with or without L-NMMA were run side by side.

2.7. Fixation/excess LDL experiments

To test the role of LDL receptors in LDL transport through BAEC monolayers, fixation or excess LDL was used to block LDL receptor mediated transcytosis. For fixation experiments, one monolayer was fixed in 1% paraformaldehyde for 10 min at 37 °C before being placed into the chamber, while the control monolayer was incubated with 1% BSA MEM under the same conditions. For excess LDL studies, 5 μg/ml DiI-LDL was added to one monolayer, and 5 μg/ml DiI-LDL plus 250 μg/ml native LDL (Biomedical Technologies, Stoughton, MA) was added to the other monolayer to saturate the LDL receptors. The two monolayers were run side by side under diffusive conditions (no hydrostatic pressure gradient).

2.8. Three-pore model

As described elsewhere (4, 24), the three pores used to model macromolecular transport across the endothelium are: transcellular/vesicles (pore 1); paracellular/breaks in the tight junction strand (pore 2); leaky junctions associated with cell turnover or death (pore 3). For a single pathway, the apparent permeability (P_e) of a solute resulting from diffusive and convective contributions can be described using the Patlak equation (30):

$$P_e = P_0 Z + J_v(1-\sigma) \quad (1)$$

where P_0 is the diffusive permeability, σ is the reflection coefficient of the solute, J_v is the water flux, and Z, which defines the relative importance of convection and diffusion, is defined as:

$$Z=\frac{N_{pe}}{e^{N_{pe}}-1} \quad (2)$$

where N_{pe} is the Peclet number,

$$N_{pe}=\frac{J_v(1-\sigma)}{P_0} \quad (3)$$

In applying this model to our data to determine the relative contribution of each pore to LDL and water transport, we assume that water can only be transported through pore 2 (J_{v2}) and pore 3 (J_{v3}). In addition, due to its large size LDL cannot go through pore 2, so it is only transported through vesicles (P_{01}) and the leaky junction (P_{03}), and σ_3 is equal to 0, since the size of leaky junction is expected to be much larger than LDL diameter (8).

With these assumptions, the three-pore model can be described by the following three equations:

$$J_v=J_{v2}+J_{v3} \quad (4)$$

$$P_e=P_0+P_{03}Z_3+J_{v3} \quad (5)$$

$$P_0=P_{01}+P_{03} \quad (6)$$

where P_{03} is the diffusive permeability of pore 3, and Z_3 is defined as above.

2.9. LDL uptake measurement

LDL uptake by BAEC monolayers was measured following a method described by Sprague et al (35). In brief, after exposure to shear or static conditions for 4 h, BAEC monolayers were rinsed with 2% BSA in DPBS at 4°C. The monolayer was washed a total of five times, the final two rinses with 10 min duration, with 2% BSA followed by one rinse with ice cold DPBS. In order to remove the surface binding DiI-LDL from the cells, 200 μl heparin at a concentration of 10 mg/ml in DPBS was added to the filter and incubated with the cells for 1 h at 4°C. Afterwards, cells on the porous filters were rinsed with DPBS for three times, and then lysed with 0.1% SDS in 0.1 N NaOH for 1 h at room temperature. The lysate combined with 3X DPBS washes were collected and used to measure the fluorescence intensity as well as the total protein using a Synergy HT multi-model microplate reader (Winooski, VT).

2.10. Statistical analysis

Data are presented as mean ± SE. Differences were assessed by using two-way ANOVA (time and treatment) and unpaired Student's t-test with $P<0.05$ considered significant. For multiple comparisons, the Bonferroni correction was used, which gives a conservative significance level of P divided by the number of comparisons.

3. Results

3.1. Effect of short term-shear stress on water flux (J_v) and LDL permeability (P_e)

Figure 1 displays the J_v responses of BAEC monolayers to an acute change in shear stress level. The J_v values were normalized by the respective baseline value for each case at 60 min, when shear stress was applied. Baseline J_v values were not significantly different between static control ($1.97 \pm 0.33 \times 10^{-6}$ cm·s^{-1}), shear ($2.27 \pm 0.23 \times 10^{-6}$ cm·s^{-1}; P>0.48 vs static), and shear + L-NMMA ($3.04 \pm 0.55 \times 10^{-6}$ cm·s^{-1}; P>0.22 vs shear). As observed in previous experiments, both the static and shear groups showed the typical "sealing" behavior in which J_v decreased continuously to its baseline value during the first 60 min of 10 cm H_2O pressure gradient application (9). The sealing effect was not affected significantly by a treatment of BAEC monolayers with 50 μM L-NMMA on the luminal side. As shown in figure 1, application of shear stress at 60 min elicited a time-dependent increase in J_v to 2.37±0.24-fold relative to its baseline, and 3.10-fold compared with the static control, after 3-h exposure to shear stress. This marked increase of J_v in response to shear stress was completely suppressed when the cells were treated with 50 μM L-NMMA, which showed no significant differences from the static control (for all time points). This indicates that shear-induced increase in water flux is mediated by a NO-dependent mechanism.

Figure 2 displays the effect of shear stress on LDL convective permeability (P_e). P_e was calculated at 1 hr intervals by determining the slope of the tracer concentration in the abluminal reservoir vs time plots within each hour interval. Similar baseline values of P_e, established during the first 60 min of pressure differential application, were obtained for static control ($4.22 \pm 0.83 \times 10^{-7}$ cm·s^{-1}), shear ($4.80 \pm 0.58 \times 10^{-7}$ cm·s^{-1}; P>0.56 vs static control), and shear plus L-NMMA ($5.58 \pm 0.80 \times 10^{-7}$ cm·s^{-1}; P>0.42 vs shear). At 60 min, the acute application of shear stress increased P_e significantly in a time-dependent manner, up to 3.00±0.46-fold at the end of 4 h (data are normalized to each baseline). As expected, LDL transport was not inhibited significantly when 50 μM L-NMMA was added. The mean value of P_e for shear plus L-NMMA monolayers shows attenuation but no significant difference relative to shear without L-NMMA cells (P>0.50). This suggests that shear induced increases of LDL transport are not mediated primarily by a NO dependent mechanism.

3.2. Effect of short term-shear stress on BAEC apoptosis

The measurements of P_e indicate that shear stress increases LDL transport through cultured BAEC monolayers. To explore whether the shear responses of P_e are due to shear induced cell apoptotic effects, we performed immunostaining of VE-cadherin and measured apoptosis using the TUNEL technique. The nuclei of apoptotic cells in Fig. 3 are stained red with TMR-red labeled dUTP incorporated into damaged DNA. Apoptotic cells were usually observed to be located in a narrow space between two or more healthy cells. As a secondary marker and to confirm the TUNEL staining, morphological hallmarks of apoptosis were identified: arrows in Fig. 3 denote condensation of nuclear material and cell shrinkage, while arrowheads denote apoptotic bodies. We found a near perfect agreement between the TUNEL staining and the morphological hallmarks of apoptosis. In addition, orthogonal views of the confocal images in Fig.3 show that most of the apoptotic cells protrude out from the monolayer as if being extruded by neighboring cells, a process that has been previously described for apoptotic epithelial cells (32). Gaps in the cell-cell junction (denoted by an asterisk in Fig. 3) formed in the vicinity of the apoptotic cells, often on the junction of a neighboring cell opposite the apoptotic cell.

Considering the uneven distribution of the shear stress over the entire filter, with maximum at the edge and minimum in the centre, we counted the apoptotic cells separately in these two areas. However the results showed no significant difference between the centre and the edge so the average over the entire filter was used. The average apoptotic rate of the static control was 2.09±0.23% (Fig. 4). 3h-shear application increased the apoptotic rate by 1.68±0.26-fold ($P < 0.01$ vs. static control). To examine whether the treatment of BAECs with L-NMMA could affect the apoptosis, we ran two experiments with or without L-NMMA side by side and then determined the apoptotic rates. As shown in figure 4, the apoptotic rate of the shear plus L-NMMA monolayers was not significantly different from the shear without L-NMMA cells (P=0.49).

3.3 Effect of short term-shear stress on LDL uptake

We measured the LDL uptake by BAEC monolayers after exposure to static or shear conditions. It is evident in Fig. 5 that the internalization of LDL at the end of 3 h shear application increased by 1.32 fold over the static control (shear: 1878 ± 446 ng/mg BAEC protein vs. static control: 1425 ± 338 ng/mg BAEC protein, $P < 0.05$).

3.4. Three-pore model

To assess the contribution of transcellular transport through vesicles to the overall LDL transport, we ran experiments on BAEC monolayers with or without fixation (side by side) for the static controls without a pressure differential to assess diffusive permeability. To further assess the transcellular transport of LDL, we incubated some monolayers with both DiI-LDL and 50-fold excess native, untagged LDL that could competitively bind to the active sites of the receptor. Table 1 shows the diffusive permeability of control (P_0) and fixed or receptor-blocked monolayers (P_{03}). The contribution of the vesicular pathway to diffusive permeability (P_{01}) was calculated from these values using equation (6). The diffusive permeability of fixed monolayers is less than those incubated with excess LDL ($P<0.05$) which suggests that a small portion of LDL could go through the cells via a non-specific vesicular mediated pathway. It should be noted that we only used receptor blocking not fixation for shear experiments since live cells are required to obtain shear responses. Shear stress application increased the diffusive permeability for both control and receptor-blocked monolayers.

Using data from Table 1 and the values of J_v and P_e obtained from the solvent drag experiments, we solved equations 4–6 to determine J_{v2}, J_{v3}, and P_{01}. Note that for the calculation of P_{01}, only the “excess LDL” data in Table 1 was used since it is available for both static and shear experiments. The parameters of the three-pore model are summarized in Table 2 along with the contributions of each pore to overall transport.

3.5. Effect of long term-shear stress on LDL permeability (P_e) and BAEC apoptosis

To examine the effect of a long time-shear exposure of BAEC monolayers on LDL transport, we extended the recording time of P_e to 12hr, then stained the VE-cadherin of the cells, and measured apoptosis using the TUNEL technique. As shown in Fig. 6A, BAECs displayed the typical cobblestone morphology for the static control and showed an elongation after shear. There are small gaps beginning to form around the apoptotic cells (arrows).

Baseline Pe values, established during the first 60 min of pressure differential application, were similar for static control and shear groups ($1.55 \pm 0.13 \times 10^{-7}$ cm/s and $1.64 \pm 0.38 \times 10^{-7}$ cm/s, respectively; $P>0.36$). However, these values are about 3-fold lower than the baselines established for the short term experiment. We hypothesize that this may be due to the timing of the experiments. Short term experiments were run on monolayers 5–7 days

post platting. At these time points, for the short term experiment, we obtained monolayers with J_v and P_e values that were within the normal range based on our previous work. However we found that older monolayers (days 6 and 7) did not remain intact for the duration of the long term experiment. For this reason, the long term experiments were always run on day 5. Earlier work in our lab (13) has shown that younger confluent monolayers display lower transport properties, most likely due to the appearance of giant cells in older monolayers.

At 60 min, the application of shear stress affected LDL permeability in a time-dependent manner, with significant increases at the end of 4 (2.24±0.54 fold), 6 (2.42±0.56 fold), and 8hr (3.25±0.95 fold) and then decreases close to the baseline level (0.87±0.26 fold)at the end of 12 hr (Fig. 6B, data are normalized to each baseline). P_e of the static control stayed at the baseline level without any significant change. Fig. 6C shows the apoptotic rates of BAEC monolayers at the beginning of each experiment and after exposure to static or shear conditions for 4hr and 12hr. The average apoptotic rate of BAEC monolayers at the beginning was 1.54±0.17% and increased insignificantly for the static control. The apoptosis of BAEC monolayers exposed to shear stress was enhanced significantly at the end of 4 h, up to 2.28±0.36 fold relative to the apoptotic rate at the beginning, and came down at the end of 12 h (shear: 1.33 ± 0.37 fold vs. static control: 1.46 ± 0.35 fold, $P>0.05$).

4. Discussion

Shear induced increases in water flux have been observed in many endothelial cell types in vitro, e.g. BAEC (7, 23, 34), BREC (20) and HUVEC (29), as well as some intact vessels in vivo (19). Several studies have shown that this phenomenon is mediated by shear induced NO release that may be related to endothelial glycocalyx and its mechanotransduction (7, 23). The present study of BAEC confirms that shear induced increase in J_v is indeed mediated by NO production, since this increase could be completely suppressed when the cells were treated with L-NMMA (Fig 1). It should be noted that the increase of J_v after 3h exposure to shear was 2.37-fold relative to the 60-min baseline value, which is somewhat lower than shear induced responses in previous studies performed on BAEC, ranging between 3.5 and 5 times the 60-min baseline value (7, 23, 34). This discrepancy may be attributed to the different sources of BAEC (Lonza vs. VEC Technologies) and levels of shear application (the maximum at the edge: 12 dyn/cm^2 vs. 20 dyn/cm^2). The maximum shear stress imposed in the present study (12 dyn/cm^2) is within the range of shear stresses that has been used in previous in vitro studies in endothelial cells and within the physiological range (16, 17, 31).

The concentration of L-NMMA used in the present study was consistent with the previous study by Chang et al (7), but there are some differences between Chang's and our treatments. They preincubated the cells with L-NMMA for one additional hour before imposing a 10 cm H_2O pressure differential, while we added L-NMMA on the luminal side of the monolayer at the beginning of the experiment. However, these two different treatments led to the same blocking effect on shear induced increases in J_v responses. It should also be noted that the L-NMMA treatment did not affect the water flux during the first 60-min sealing period (Fig. 1). Previous studies (9, 10) in our lab have demonstrated that sealing is driven by the transmural flow through the intercellular junctions induced by the pressure gradient and involves the recruitments of zonula occludens-1 along the microtubules to the tight junction area of the cells which is NO independent.

Previous animal studies using the rabbit aorto-iliac bifurcation both in vivo (2) and ex vivo (12) have shown that the incorporation and degradation rates of LDL vary with different hemodynamic forces. Very recently, Olgac et al. (28) computed the transport of LDL in a

three-dimensional, patient-specific model of a human left coronary artery where the endothelium was represented by a shear stress-dependent, three pore model, taking into account the LDL passage through leaky junctions, and the vesicular pathway. They confirmed the relationship between high-LDL accumulation and actual plaque locations where flow recirculation and low wall shear stress were present. The success of their model hinged on the assumption that the leaky junction (pore 3) was dependent on apoptosis that was reduced with increasing shear stress. However, in vitro studies of the effects of shear stress on LDL permeability under well defined and controlled conditions have not been reported previously.

The baseline values of both convective and diffusive permeability measured in the present study are close to those measured by Cancel et al (4). Results in Fig. 2 show that shear stress application initiated a time-dependent increase in endothelial permeability to LDL, up to 3.00±0.46-fold of the baseline value at the end of 3 hours of shear. This shear induced increase in permeability of macromolecules is consistent with one previous study performed in vitro to measure the permeability of bovine serum albumin under physiological levels of shear stress (17). It should be noted that a step change in shear stress from a static condition is not typical of normal arterial physiology in vivo, but might occur in pathological situations such as ischemia-reperfusion (14). Moreover, results in Fig. 6B demonstrate that application of shear stress for a longer time (12h) reduced the endothelial permeability to LDL even lower than the baseline value (0.87±0.26 fold). This phenomenon is consistent with the observation in the fully shear adapted cardiovascular system in vivo, that atherosclerosis and enhanced LDL uptake occur preferentially in regions of low and oscillatory shear and not in stable streamline flow regions of higher shear stress (37)

It should be noted that the apoptotic rate of our controls (1.54±0.17%) is higher than in a previous study performed by Cancel et al. (5), where the baseline apoptotic rate was 0.3 ± 0.036%. Again, different cell sources for BAEC are likely to account for the differences in growth and death behavior. The apoptotic level induced by 3h-shear application (Fig. 4 and Fig. 6C) is similar to that observed in the same Lonza BAEC by Rennier et al (31). This group exposed BAEC to 12 dyn/cm^2 for 6 h and investigated the effects of shear stress and tumor necrosis factor alpha (TNFα) on endothelial apoptosis. They found that TNFα induced a two-fold increase in apoptotic cells over control while 6h of shear stress alone increased the apoptotic rates by 1.5 fold over the static control condition. Results in Fig. 6C show that the apoptotic rate of BAEC monolayers at the end of 12hr shear experiment was not significantly different from the static control. This observation is consistent with a previous study by Hu et al (16). They studied the effect of colchicine and shear stress on BAEC apoptosis and found that the treatment of colchicine could induce a sustained c-Jun NH2-terminal kinase (JNK) activation and cell apoptosis, while the exposure to shear stress alone for 8 hrs did not induce apoptosis. Two other studies examined the effect of long term (18hrs) shear stress on TNFα (11) or H_2O_2 (15) induced endothelial cell apoptosis. Both of these studies found that shear suppressed TNFα or H_2O_2 induced apoptosis, and that this effect could be attenuated by the NO synthase inhibitor L-NMMA. In the present study, we found that L-NMMA treatment had a small, but not statistically significant, effect in reducing shear induced increases in EC apoptosis (Figure 4), and a larger, but still insignificant effect in reducing shear induced LDL permeability (Figure 2). Taken together these results suggest that the time scale of shear stress application leads to different effects on endothelial apoptosis behavior – shorter exposures to shear inducing apoptosis and longer exposures suppressing apoptosis.

The predictions of our three-pore model, summarized in Table 2, indicate that pore 3 (leaky junction) is the dominant pathway for LDL transport but pore 2 (break in the tight junction strand) carries most of the water. These predictions are consistent with in vitro models of

BAEC (4) and BREC (24) reported before. A previous in vivo study by Wiklund et al. (40), using methylated LDL to block its recognition by the LDL receptor and comparing the influx rates of both kinds of LDL (methylated and native), has also shown that the influx of LDL into the aorta is not significantly dependent on the LDL receptor, implying other mechanisms are involved.

Shear stress enhances the pore 2 contribution to water flux (shear: 78% vs. static: 61%) and this could be blocked by L-NMMA treatments of BAEC monolayers (shear: 78% vs. shear + L-NMMA: 58%), which confirms the important role of NO in shear induced J_v responses. Although the relative contributions of pore 1 (vesicles) and pore 3 to LDL transport show no significant difference between static and shear groups, shear indeed increases the values of P_e and P_0. As discussed above, shear induced leaky junctions forming around apoptotic cells are the main cause of the enhanced LDL transport. Moreover, shear also increased the vesicular transport of LDL, which is consistent with our LDL uptake measurements (figure 5) as well as previous uptake studies performed on BAECs (26, 35) and HUVECs (18). Another prediction from the three-pore model indicates that there is no significant difference in pore contributions to LDL transport between shear treatment groups with and without L-NMMA. This is consistent with our observations that L-NMMA had no significant effect on LDL P_e (figure 2) and apoptosis rate (figure 4).

In conclusion, this was the first in vitro study to measure shear effects on hydraulic conductivity and LDL permeability simultaneously. Our results for Lp are consistent with previous reports indicating that an acute change in shear stress (from zero to a steady level) induces an increase in water flux that is mediated by a NO dependent mechanism. Our results for Pe suggest that the permeability of endothelial monolayers to LDL is enhanced by a short term-shear application and reduced nearly to the baseline level by a longer time-shear exposure, positively correlated to the leaky junctions forming around apoptotic cells.

Acknowledgments

The authors thank Sparkle Russell and Dr. Sandra V. Lopez-Quintero for providing help on the shear system.

Grants

This work was supported by NIH Grant HL57093 and Grants-in-Aid from the National Natural Science Foundation of China (No.11072023).

References

1. Adamson RH, Sarai RK, Altangerel A, Clark JF, Weinbaum S, Curry FE. Microvascular permeability to water is independent of shear stress, but dependent on flow direction. Am J Physiol Heart Circ Physiol. 2013; 304:H1077–1084. [PubMed: 23417864]
2. Berceli SA, Warty VS, Sheppeck RA, Mandarino WA, Tanksale SK, Borovetz HS. Hemodynamics and low density lipoprotein metabolism. Rates of low density lipoprotein incorporation and degradation along medial and lateral walls of the rabbit aorto-iliac bifurcation. Arteriosclerosis. 1990; 10:686–694. [PubMed: 2403296]
3. Buchanan JR Jr, Kleinstreuer C, Truskey GA, Lei M. Relation between non-uniform hemodynamics and sites of altered permeability and lesion growth at the rabbit aorto-celiac junction. Atherosclerosis. 1999; 143:27–40. [PubMed: 10208478]
4. Cancel LM, Fitting A, Tarbell JM. In vitro study of LDL transport under pressurized (convective) conditions. Am J Physiol Heart Circ Physiol. 2007; 293:H126–132. [PubMed: 17322415]
5. Cancel LM, Tarbell JM. The role of apoptosis in LDL transport through cultured endothelial cell monolayers. Atherosclerosis. 2010; 208:335–341. [PubMed: 19709659]
6. Cancel LM, Tarbell JM. The role of mitosis in LDL transport through cultured endothelial cell monolayers. Am J Physiol Heart Circ Physiol. 2011; 300:H769–776. [PubMed: 21169397]

7. Chang YS, Yaccino JA, Lakshminarayanan S, Frangos JA, Tarbell JM. Shear-induced increase in hydraulic conductivity in endothelial cells is mediated by a nitric oxide-dependent mechanism. Arterioscler Thromb Vasc Biol. 2000; 20:35–42. [PubMed: 10634798]
8. Chen YL, Jan KM, Lin HS, Chien S. Ultrastructural studies on macromolecular permeability in relation to endothelial cell turnover. Atherosclerosis. 1995; 118:89–104. [PubMed: 8579635]
9. DeMaio L, Chang YS, Gardner TW, Tarbell JM, Antonetti DA. Shear stress regulates occludin content and phosphorylation. Am J Physiol Heart Circ Physiol. 2001; 281:H105–113. [PubMed: 11406474]
10. DeMaio L, Tarbell JM, Scaduto RC Jr, Gardner TW, Antonetti DA. A transmural pressure gradient induces mechanical and biological adaptive responses in endothelial cells. Am J Physiol Heart Circ Physiol. 2004; 286:H731–741. [PubMed: 14527936]
11. Dimmeler S, Haendeler J, Nehls M, Zeiher AM. Suppression of apoptosis by nitric oxide via inhibition of interleukin-1beta-converting enzyme (ICE)-like and cysteine protease protein (CPP)-32-like proteases. J Exp Med. 1997; 185:601–607. [PubMed: 9034139]
12. Ding Z, Fan Y, Deng X, Sun A, Kang H. 3,3′-Dioctadecylindocarbocyanine-low-density lipoprotein uptake and flow patterns in the rabbit aorta-iliac bifurcation under three perfusion flow conditions. Exp Biol Med (Maywood). 2010; 235:1062–1071. [PubMed: 20705630]
13. Dull RO, Jo H, Sill H, Hollis TM, Tarbell JM. The effect of varying albumin concentration and hydrostatic pressure on hydraulic conductivity and albumin permeability of cultured endothelial monolayers. Microvasc Res. 1991; 41:390–407. [PubMed: 2072871]
14. Han J, Zern BJ, Shuvaev VV, Davies PF, Muro S, Muzykantov V. Acute and chronic shear stress differently regulate endothelial internalization of nanocarriers targeted to platelet-endothelial cell adhesion molecule-1. ACS Nano. 2012; 6:8824–8836. [PubMed: 22957767]
15. Hermann C, Zeiher AM, Dimmeler S. Shear stress inhibits H2O2-induced apoptosis of human endothelial cells by modulation of the glutathione redox cycle and nitric oxide synthase. Arterioscler Thromb Vasc Biol. 1997; 17:3588–3592. [PubMed: 9437209]
16. Hu YL, Li S, Shyy JY, Chien S. Sustained JNK activation induces endothelial apoptosis: studies with colchicine and shear stress. Am J Physiol. 1999; 277:H1593–1599. [PubMed: 10516199]
17. Jo H, Dull RO, Hollis TM, Tarbell JM. Endothelial albumin permeability is shear dependent, time dependent, and reversible. Am J Physiol. 1991; 260:H1992–1996. [PubMed: 1905493]
18. Kang H, Fan Y, Sun A, Deng X. Compositional or charge density modification of the endothelial glycocalyx accelerates flow-dependent concentration polarization of low-density lipoproteins. Exp Biol Med (Maywood). 2011; 236:800–807. [PubMed: 21659384]
19. Kim MH, Harris NR, Tarbell JM. Regulation of capillary hydraulic conductivity in response to an acute change in shear. Am J Physiol Heart Circ Physiol. 2005; 289:H2126–2135. [PubMed: 15994851]
20. Lakshminarayanan S, Gardner TW, Tarbell JM. Effect of shear stress on the hydraulic conductivity of cultured bovine retinal microvascular endothelial cell monolayers. Curr Eye Res. 2000; 21:944–951. [PubMed: 11262618]
21. Lin SJ, Jan KM, Chien S. Role of dying endothelial cells in transendothelial macromolecular transport. Arteriosclerosis. 1990; 10:703–709. [PubMed: 1698353]
22. Lin SJ, Jan KM, Weinbaum S, Chien S. Transendothelial transport of low density lipoprotein in association with cell mitosis in rat aorta. Arteriosclerosis. 1989; 9:230–236. [PubMed: 2923579]
23. Lopez-Quintero SV, Amaya R, Pahakis M, Tarbell JM. The endothelial glycocalyx mediates shear-induced changes in hydraulic conductivity. Am J Physiol Heart Circ Physiol. 2009; 296:H1451–1456. [PubMed: 19286951]
24. Lopez-Quintero SV, Ji XY, Antonetti DA, Tarbell JM. A three-pore model describes transport properties of bovine retinal endothelial cells in normal and elevated glucose. Invest Ophthalmol Vis Sci. 2011; 52:1171–1180. [PubMed: 21357410]
25. Michel CC, Curry FE. Microvascular permeability. Physiol Rev. 1999; 79:703–761. [PubMed: 10390517]
26. Niwa K, Kado T, Sakai J, Karino T. The effects of a shear flow on the uptake of LDL and acetylated LDL by an EC monoculture and an EC-SMC coculture. Ann Biomed Eng. 2004; 32:537–543. [PubMed: 15117027]

27. Olgac U, Kurtcuoglu V, Poulikakos D. Computational modeling of coupled blood-wall mass transport of LDL: effects of local wall shear stress. Am J Physiol Heart Circ Physiol. 2008; 294:H909–919. [PubMed: 18083898]
28. Olgac U, Poulikakos D, Saur SC, Alkadhi H, Kurtcuoglu V. Patient-specific three-dimensional simulation of LDL accumulation in a human left coronary artery in its healthy and atherosclerotic states. Am J Physiol Heart Circ Physiol. 2009; 296:H1969–1982. [PubMed: 19329764]
29. Pang Z, Antonetti DA, Tarbell JM. Shear stress regulates HUVEC hydraulic conductivity by occludin phosphorylation. Ann Biomed Eng. 2005; 33:1536–1545. [PubMed: 16341921]
30. Patlak CS, Goldstein DA, Hoffman JF. The flow of solute and solvent across a two-membrane system. J Theor Biol. 1963; 5:426–442. [PubMed: 5875168]
31. Rennier K, Ji JY. Shear stress regulates expression of death-associated protein kinase in suppressing TNFalpha-induced endothelial apoptosis. J Cell Physiol. 2012; 227:2398–2411. [PubMed: 21826654]
32. Rosenblatt J, Raff MC, Cramer LP. An epithelial cell destined for apoptosis signals its neighbors to extrude it by an actin- and myosin-dependent mechanism. Curr Biol. 2001; 11:1847–1857. [PubMed: 11728307]
33. Schwenke DC, Carew TE. Initiation of atherosclerotic lesions in cholesterol-fed rabbits. II. Selective retention of LDL vs. selective increases in LDL permeability in susceptible sites of arteries. Arteriosclerosis. 1989; 9:908–918. [PubMed: 2590068]
34. Sill HW, Chang YS, Artman JR, Frangos JA, Hollis TM, Tarbell JM. Shear stress increases hydraulic conductivity of cultured endothelial monolayers. Am J Physiol. 1995; 268:H535–543. [PubMed: 7532373]
35. Sprague EA, Steinbach BL, Nerem RM, Schwartz CJ. Influence of a laminar steady-state fluid-imposed wall shear stress on the binding, internalization, and degradation of low-density lipoproteins by cultured arterial endothelium. Circulation. 1987; 76:648–656. [PubMed: 3621525]
36. Tarbell JM. Mass transport in arteries and the localization of atherosclerosis. Annu Rev Biomed Eng. 2003; 5:79–118. [PubMed: 12651738]
37. Tarbell JM. Shear stress and the endothelial transport barrier. Cardiovasc Res. 2010; 87:320–330. [PubMed: 20543206]
38. Traore M, Sun RJ, Fawzi-Grancher S, Dumas D, Qing X, Santus R, Stoltz JF, Muller S. Kinetics of the endocytotic pathway of Low Density Lipoprotein (LDL) in human endothelial cells line under shear stress: an in vitro confocal microscopy study. Clin Hemorheol Microcirc. 2005; 33:243–251. [PubMed: 16215290]
39. Weinbaum S, Tzeghai G, Ganatos P, Pfeffer R, Chien S. Effect of cell turnover and leaky junctions on arterial macromolecular transport. Am J Physiol. 1985; 248:H945–960. [PubMed: 4003572]
40. Wiklund O, Carew TE, Steinberg D. Role of the low density lipoprotein receptor in penetration of low density lipoprotein into rabbit aortic wall. Arteriosclerosis. 1985; 5:135–141. [PubMed: 3977773]
41. Williams DA. Network assessment of capillary hydraulic conductivity after abrupt changes in fluid shear stress. Microvasc Res. 1999; 57:107–117. [PubMed: 10049659]

Highlights

We measured shear induced water and LDL fluxes across cultured BAEC monolayers.

We developed a three-pore model to describe the transport dynamics.

An acute change in shear stress increases water flux that are mediated by NO.

LDL flux is enhanced by a 3h-shear application and reduced by a 12h-shear exposure.

LDL transport is positively correlated to the leaky junctions around apoptotic cells.

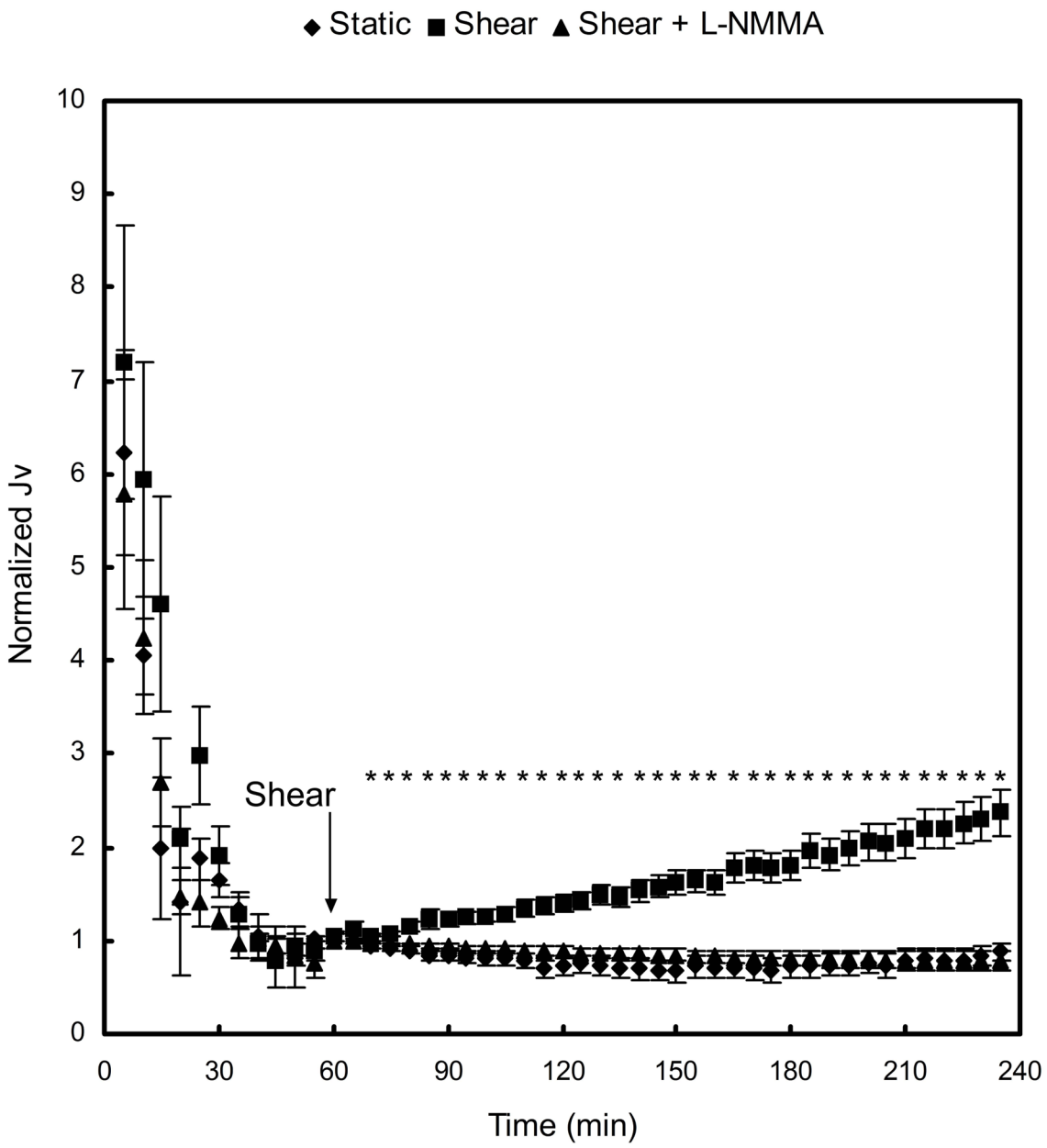

Fig. 1.

Effect of short term-shear stress on water flux (J_v). At time 0 min, a hydrostatic pressure differential of 10 cm H_2O was applied, and a baseline was established after 60 min. Application of shear stress at 60 min triggered a time-dependent increase in J_v, which was blocked by a treatment of BAEC monolayers with 50 μM L-NMMA. Baseline J_v for static control, shear, and shear + L-NMMA were 1.97 ± 0.33 $\times 10^{-6}$ cm·s^{-1} (n=7), 2.27 ± 0.23 $\times 10^{-6}$ cm·s^{-1} (n=7), and 3.04 ± 0.55 $\times 10^{-6}$ cm·s^{-1} (n=7), respectively. * $P < 0.05$, significant differences between shear and static monolayers. Data are presented as mean ± SEM.

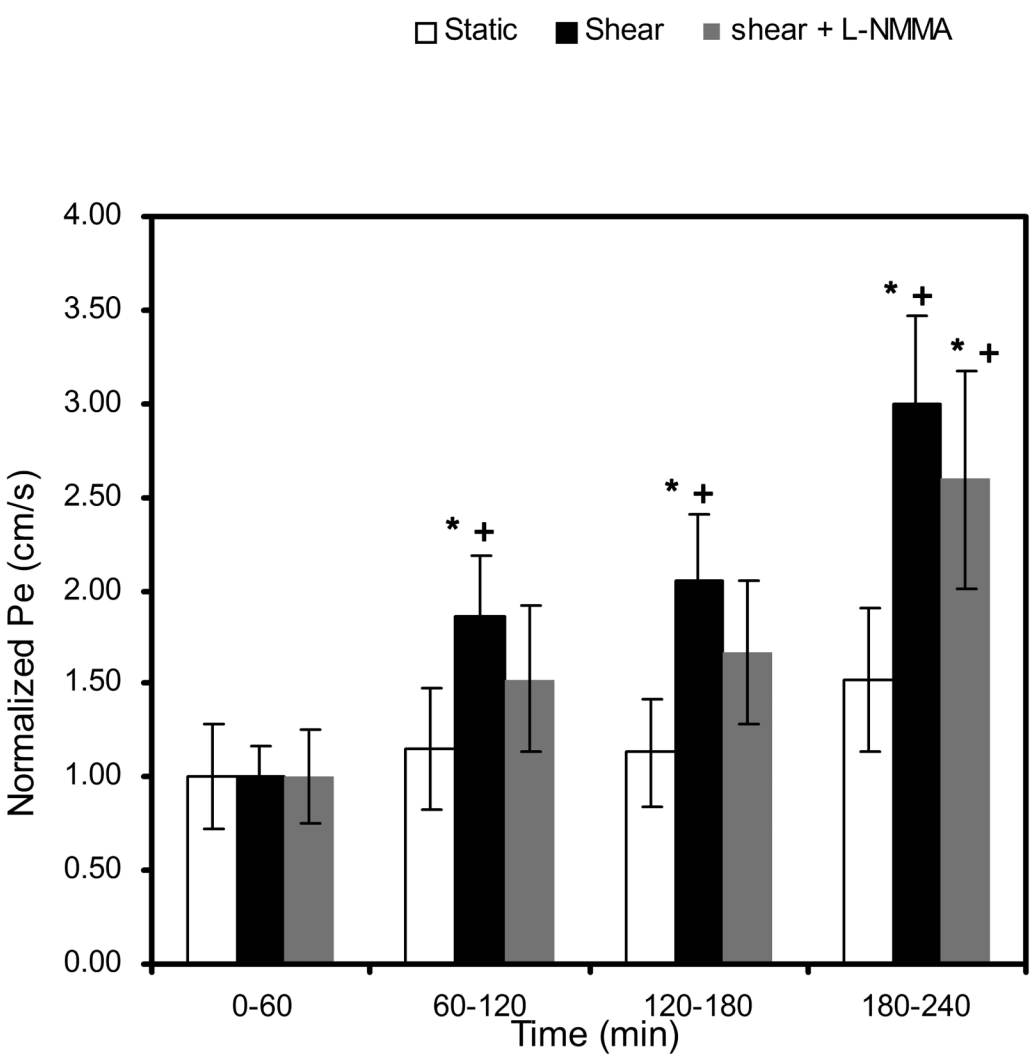

Fig. 2.

Effect of short term-shear stress on LDL permeability (P_e). Application of shear stress at 60 min elicited a time-dependent increase in P_e. This marked increase cannot be significantly blocked by a treatment of BAECs with 50 μM L-NMMA (P>0.999 vs. shear). Baseline P_e for static control, shear, and shear + L-NMMA were 4.22 ± 0.83 $\times 10^{-7}$ cm·s^{-1} (n=8), 4.80 ± 0.58 $\times 10^{-7}$ cm·s^{-1} (n=12), and 5.58 ± 0.80 $\times 10^{-7}$ cm·s^{-1} (n=9), respectively. * P < 0.01, significant differences compared to the baseline value for each case at 60 min. + P < 0.01, significant differences compared to the static control within each hour interval. Data are presented as mean ± SEM.

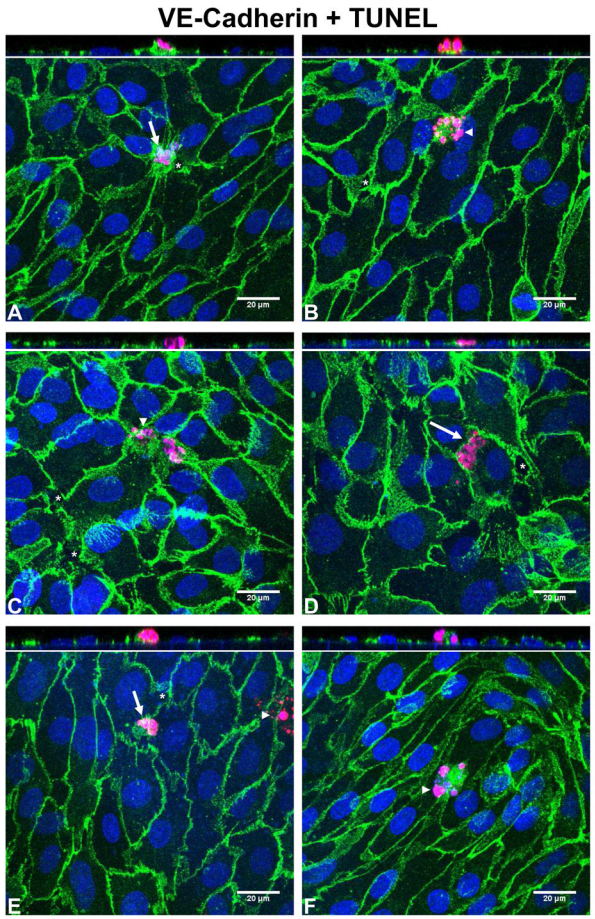

Fig. 3.

Representative confocal photomicrographs of BAEC monolayers stained with VE-cadherin (green), DAPI (nucleus; blue), and TUNEL (apoptosis marker; red). As a secondary marker, morphological hallmarks of apoptosis were identified: arrows denote condensation of nuclear material and cell shrinkage, arrowheads denote apoptotic bodies. Gaps in the cell-cell junction (denoted by an asterisk) formed in the vicinity of the apoptotic cells, often on the junction of a neighboring cell opposite the apoptotic cell. (A) and (B) static control; (C) and (D) shear; (E) and (F) shear + L-NMMA. The orthogonal XZ views go across the apoptotic cell in each image.

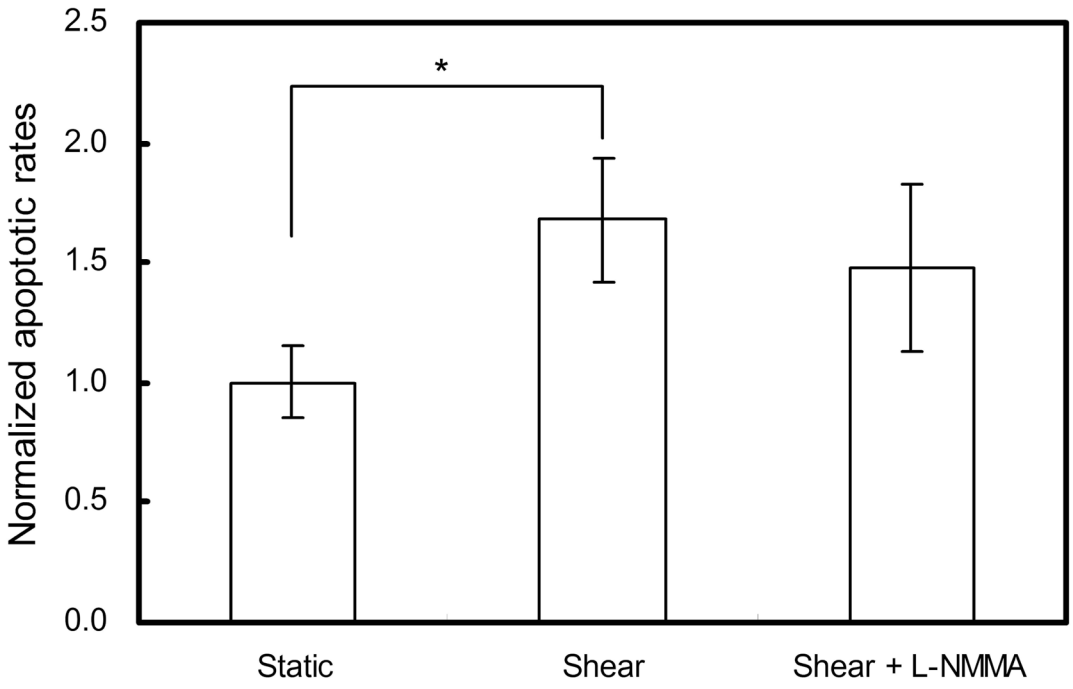

Fig. 4.

Effect of short term-shear stress on the apoptosis rate of BAEC monolayers. 3h-shear application enhanced apoptosis significantly (n=6). * $P < 0.01$, significant differences between shear and static monolayers. Data are presented as mean ± SEM.

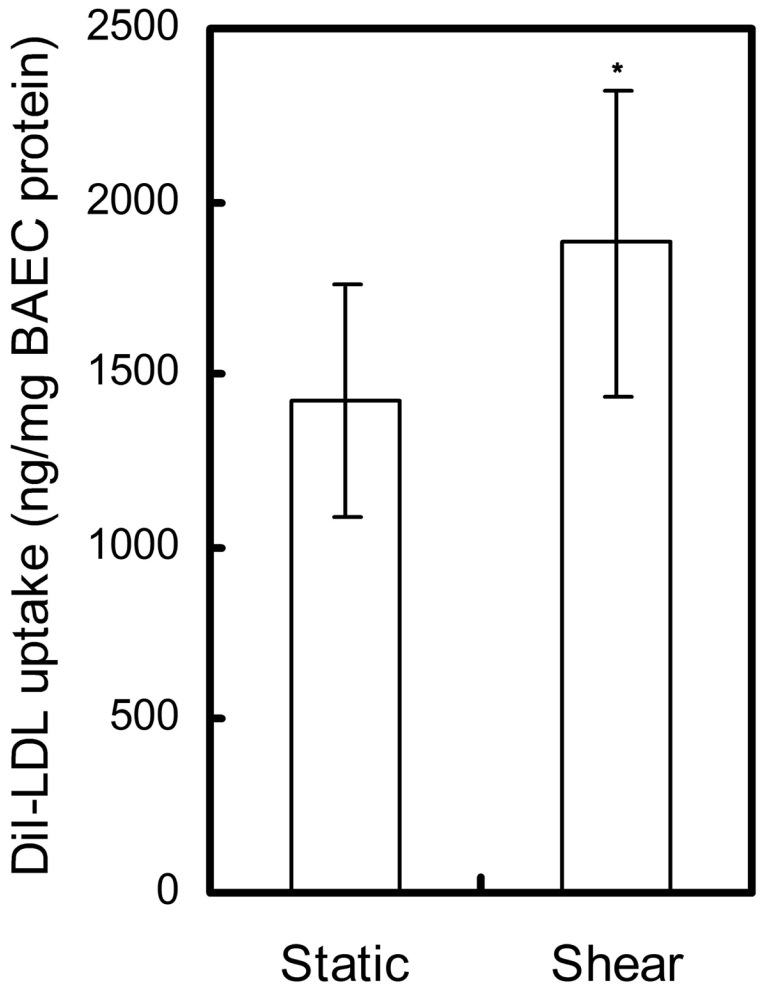

Fig. 5.
Effect of short term-shear stress on the uptake of LDL by BAEC monolayers. * $P < 0.05$, significant differences between shear and static monolayers. Data are presented as mean ± SEM.

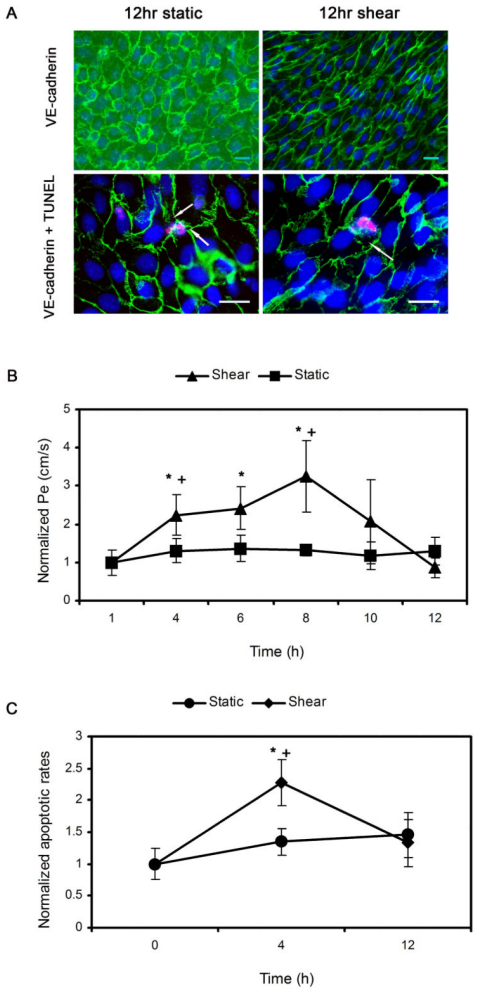

Fig. 6.

A: Fluorescence microscopy images of BAEC monolayers after VE-cadherin (top) and TUNEL staining (bottom) for 12hr static control and 12hr shear group. Scale bar is 20 μm. Arrows denote gaps around apoptotic cells. B: Effect of long time-shear application on LDL permeability (P_e). Baseline P_e for static control and shear were $1.55 \pm 0.13 \times 10^{-7}$ cm·s^{-1} (n=4) and $1.64 \pm 0.38 \times 10^{-7}$ (n=4) cm·s^{-1}, respectively. * $P < 0.05$, significant differences compared to the baseline value for each case at 60 min. + $P < 0.05$, significant differences compared to the static control within each hour interval. Data are normalized to each baseline and presented as mean ± SEM. C: Effect of long time-shear application on cell apoptosis. The apoptotic rate of the cells at the beginning of each experiment was 1.54±0.17%. * $P < 0.05$, significant differences compared to the value at time zero. + $P < 0.05$, significant differences compared to the static control at the end of 4 h. Data are normalized to the apoptotic rate at time zero and presented as mean ± SEM.

Table 1

LDL diffusive permeability of fixed and receptor-blocked BAEC monolayers

Expt. set	n	P_0, cm/s $\times 10^{-7}$	P_{03}, cm/s $\times 10^{-7}$	P_{01}, cm/s $\times 10^{-7}$
Static, fixation	8	2.12 ± 0.36	0.66 ± 0.04	1.46
Static, excess LDL	5	2.03 ± 0.28	0.86 ± 0.08	1.17
Shear, excess LDL	8	4.60 ± 0.70	2.45 ± 0.44	2.15

P_0: the diffusive permeability of control; P_{03}: the diffusive permeability of fixed/receptor-blocked (P_{03}) monolayers; P_{01}: the diffusive permeability of the vesicular pathway. Data are presented as Mean ± SEM.

Table 2

Summary of three-pore model predictions

Expt. set				Pore contribution to overall transport			
				Water		LDL	
	J_v	P_e	P_0	J_{v2}	J_{v3}	vesicles	Pore 3
Static	1.74	0.80	0.21	1.06 (61%)	0.68 (39%)	0.12 (15.0%)	0.68 (85.0%)
Shear	5.38	1.42	0.46	4.18 (78%)	1.20 (22%)	0.22 (15.5%)	1.20 (84.5%)
Shear+ L-NMMA	2.40	1.23	0.46	1.40 (58%)	1.00 (42%)	0.22 (17.9%)	1.01 (82.1%)

Water and LDL permeability are given in units of $\times 10^{-6}$ cm/s. Vesicular transport was calculated on the basis of "excess LDL" experiments in Table 1. Each pore contribution was presented as the percentage to the overall transport.